19th Australasian Fluid Mechanics Conference
Melbourne, Australia
8-11 December 2014

Unsteady Boundary Layer Flow and Heat Transfer over a Permeable Shrinking Sheet with Non-Uniform Heat Source

M.M. Rahman[1] and I. Pop[2]

[1]Department of Mathematics and Statistics, College of Science
Sultan Qaboos University, PO Box 36, PC 123 Al-Khod, Muscat, Sultanate of Oman

[2]Department of Mathematics, Faculty of Mathematics and Computer Science
Babeş-Bolyai University, 400084 Cluj-Napoca, Romania

Abstract

In this paper we investigate theoretically the unsteady boundary layer flow and heat transfer over a permeable shrinking sheet with non-uniform heat source. The nondimensional governing equations have been solved numerically using the bvp4c function from Matlab for different values of the pertinent parameters; shrinking parameter λ, suction parameter S, unsteadiness parameter β, space dependent heat source parameter A, and temperature dependent heat source parameter B, keeping Prandtl number Pr fixed. Numerical results are obtained for the reduced skin-friction and heat transfer and for the velocity and temperature profiles. The results indicate that dual solutions exist for a shrinking ($\lambda < 0$) sheet for certain values of the parameter space. The results show that unsteadiness significantly controls the flow and heat transfer characteristics.

Introduction

During the past few decades, the analysis of boundary layer flow of viscous fluids due to stretching/shrinking surfaces has important applications in engineering processes and polymer industry. Examples of such technological processes concerning polymers include cooling of continuos strips or filaments, glass blowing, continuos stretching of plastic films, artificial fibres, continuos casting of metals and spinning of fibers, hot rolling, wire drawing, glass fibre, paper production, etc. Crane [1] was the first who has studied the viscous fluid subject to a stretching surface. He obtained an exact and closed form similarity solution. Gupta and Gupta [2] discussed the heat and mass transfer due to a porous stretching sheet. They presented the analysis for both suction and blowing cases. Banks [3] presented a class of similarity solutions depending upon a parameter for the boundary layer equations due to a stretching wall. The existence and uniqueness of stretching flow is discussed by Mecleod and Rajagopal [4]. In recent years, the Crane's problem [1] is extended to discuss the various aspects of the flow and heat transfer characteristics with linear and power-law surface velocities by many authors (Liao and Pop [5], Ishak et al. [6]). The review paper by Wang [7] presents comprehensive discussions of the published work on similarity stretching exact solutions of the Navier–Stokes equations. Further, it seems that Miklavčič and Wang [8] are the first who have studied the shrinking sheet problem, where the velocity on the boundary is towards a fixed point. From physical grounds vorticity of the shrinking sheet is not confined within a boundary layer, and the flow is unlikely to exist unless adequate suction on the boundary is imposed. This new type of shrinking sheet flow is essentially a backward flow as discussed by Goldstein [9]. The flow induced by a shrinking sheet shows physical phenomena quite distinct from the forward stretching flow.

The unsteady viscous flow over a stretching/shrinking surface has been also studied by several authors and we mention here Surma Devi et al. [10] and Fang et al. [11]. Zheng et al. [12] have studied the boundary layer flow and heat transfer on a permeable unsteady stretching sheet with non-uniform heat source/sink. The analytic solutions are obtained by using suitable similarity transformations and homotopy analysis method (HAM). The effects of unsteadiness parameter, Prandtl number and heat source/sink parameter on the flow and heat transfer characteristics are analyzed and discussed. The purpose of the present paper is to extend the paper by Zheng et al. [12] to the case of a shrinking sheet. Numerical techniques are used to solve the similarity equations for different values of the governing parameters. Results show that multiple (dual) solutions exist for a certain range of mass suction and unsteadiness parameters. Quite different flow behaviour is observed for an unsteady shrinking sheet from an unsteady stretching sheet. To our best of knowledge this problem has not been considered before, so that the reported results are new and original.

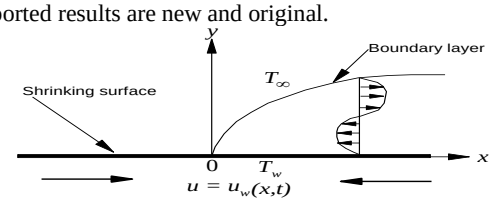

Figure 1. Geometry of the problem

Basic Equations

Consider a two-dimensional boundary layer flow over an unsteady continuously shrinking sheet in a quiescent viscous and incompressible fluid, as is shown in Fig. 1, where x and y are Cartesian coordinates measured along the shrinking surface and normal to it, respectively. It is assumed that the stretching/shrinking velocity is $u_w = \lambda U_w(x,t)$, where λ is a constant with $\lambda > 0$ corresponds to a stretching sheet and $\lambda < 0$ corresponds to a shrinking sheet, respectively. The surface temperature and the mass transfer velocity are $T_w(x,t)$ and $v_w(x,t)$, which will be defined later. Under the boundary layer assumption, the basic equations of this problem can be written as (see Zheng et al. [12])

$$\frac{\partial u}{\partial x} + \frac{\partial v}{\partial y} = 0 \tag{1}$$

$$\frac{\partial u}{\partial t} + u\frac{\partial u}{\partial x} + v\frac{\partial u}{\partial y} = \nu\frac{\partial^2 u}{\partial y^2} \tag{2}$$

$$\frac{\partial T}{\partial t} + u\frac{\partial T}{\partial x} + v\frac{\partial T}{\partial y} = \frac{k}{\rho C_p}\frac{\partial^2 T}{\partial y^2} - \frac{q'''}{\rho C_p} \tag{3}$$

with the initial and boundary conditions

$$\left.\begin{aligned} &t<0: v=u=0, T=T_\infty \text{ for any } x, y\\ &t\geq 0: v=v_w(x,t), u=u_w(x,t)=\lambda U_w(x,t),\\ &T=T_w(x,t) \text{ at } y=0\\ &u(x,t)\to 0,\ T(x,t)\to T_\infty \text{ as } y\to\infty \end{aligned}\right\} \quad (4)$$

where u and v are the velocity components along the $x-$ and $y-$ axes, T is the fluid temperature, t is time, k is the thermal conductivity, ν is the kinematic viscosity, ρ is the density, T_∞ is the constant temperature of the ambient fluid and C_p is the specific heat at constant pressure.

In order that Eqs. (1) to (3) subject to the initial and boundary conditions (4) admit similarity solutions, we assume that $u_w(x,t)$, $v_w(x,t)$, $T(x,t)$ and $q'''(x,t)$ have the following form

$$u_w(x,t)=\frac{ax}{1-\alpha t}, v_w(x,t)=-S\sqrt{\frac{a\nu}{1-\alpha t}}, T(x,t)=T_\infty+\frac{T_0 x}{1-\alpha t}$$
$$q'''(x,t)=\left(\frac{kU_w}{x\nu}\right)\left[A(T_w-T_\infty)f'+B(T-T_\infty)\right] \quad (5)$$

where a is a positive constant, α is a parameter showing the unsteadiness of the problem, S is the mass transfer parameter, with $S>0$ for suction and $S<0$ for injection, respectively, A is the coefficient of the space-dependent and B is temperature-dependent heat source or sink parameter. Note that $A<0, B<0$ correspond to internal heat sink, and $A>0, B>0$ correspond to internal heat source. Having in view (5), we assume that the following similarity variables can be considered:

$$\psi(x,y,t)=x\sqrt{a\nu/(1-\alpha t)}\, f(\eta),$$
$$T(x,y,t)=\frac{bx}{1-\alpha t}\,\theta(\eta), \eta=y\sqrt{a/\nu(1-\alpha t)} \quad (6)$$

where ψ is the stream function, which is defined in the usual way as $u=\partial\psi/\partial y$ and $v=-\partial\psi/\partial x$.

Substituting (6) into Eqs. (2) and (3), we get the following ordinary differential equations

$$f'''+ff''-f'^2-\beta\left(f'+\frac{\eta}{2}f''\right)=0 \quad (7)$$

$$\theta''+\Pr\left[f\theta'-f'\theta-\beta\left(\theta+\frac{\eta}{2}\theta'\right)\right]+Af'+B\theta=0 \quad (8)$$

subject to the boundary conditions

$$f(0)=S,\quad f'(0)=\lambda,\quad \theta(0)=1$$
$$f'(\eta)\to 0,\quad \theta(\eta)\to 0 \quad \text{as} \quad \eta\to\infty \quad (9)$$

where primes denote differentiation with respect to η and $\beta=\alpha/a$ is the unsteadiness parameter. For the present work, we assume a decelerating shrinking sheet with $\beta\leq 0$.

The physical quantities of interest are the skin friction coefficient C_f and the local Nusselt number Nu_x, which are defined as

$$C_f=\tau_w/\rho U_w^2,\quad Nu_x=xq_w/k(T_w-T_\infty) \quad (10)$$

where τ_w is the skin friction or shear stress along the surface of the sheet and q_w is the heat flux from the surface of the sheet, which are given by

$$\tau_w=\mu\left(u_y\right)_{y=0},\quad q_w=-k\left(T_y\right)_{y=0} \quad (11)$$

Using the similarity variables (6), we obtain

$$\mathrm{Re}_x^{1/2}C_f=f''(0),\quad \mathrm{Re}_x^{-1/2}Nu_x=-\theta'(0) \quad (12)$$

where $\mathrm{Re}_x=U_w x/\nu$ is the local Reynolds number.

Numerical Techniques

Following Rahman et al. [13-14], the system of ordinary differential equations (7)-(8) subject to the boundary conditions (9) are solved numerically using the function bvp4c from Matlab for different values of the parameters The numerical simulations are carried out for various values of the physical parameters such as shrinking parameter λ, suction parameter S, unsteadiness parameter β, space dependent heat source parameter A, temperature dependent heat source parameter B and Prandtl number Pr. Because of almost lack of the experimental data, the choice of the values of the parameters was dictated by the values chosen by previous investigators. The value of the Prandtl number is set equal to 0.71 which corresponds to air at room temperature, throughout the paper unless otherwise specified. The values of the other parameters are mentioned in the description of the respective figures. The code bvp4c is developed using finite difference method that implements the three-stage Lobatto IIIa formula, which is a collocation method with forth-order accuracy. In this approach, the ordinary differential equations (7)-(8) are reduced to a system of first-order by introducing new variables. The mesh selection and error control are based on the residual of the continuous solution. The relative error tolerance has been set to 10^{-7}. Because the present problem may have more than one solution (dual, upper and lower branch solutions), a 'good' initial guess is necessary. The 'infinity' $\eta\to\infty$ in the boundary condition (9) is replaced by a finite value $\eta=\eta_\infty$. We started the computation at small value, for example, $\eta=5$, then subsequently increased the value of η until the boundary conditions are verified. In this method, we have chosen a suitable finite value of $\eta\to\infty$, namely $\eta=\eta_\infty=20$ for the upper branch (first) solution and $\eta=\eta_\infty$ in the range 40-60 for the lower branch (second) solution. Examples of solving boundary value problems by bvp4c can be found in the book by Shampine et al. [15].

We notice that Eq. (7) subject to the boundary conditions (9) reduce to Eq. (6) from Fang et al. [16] when $\lambda=-1$ (shrinking sheet). We also notice that Eq. (8) subject to the boundary conditions (9) reduce to Eq. (9) from Zheng et al. [12] when $\lambda=1$. It is good to mention that Eq. $f'''+ff''-f'^2=0$ together with the boundary conditions $f(0)=0$, $f'(0)=1$, $f'(\infty)=0$ possess exact solution $f(\eta)=1-e^{-\eta}$ (Vajravelu [16]) that is unique. At $\eta=0$, $f''(0)=-1$ that exactly matches with our calculated value when $\beta=0$ in Eq. (7) and $S=0$, $\lambda=1$ in Eq. (9). It can further be noted that for $\beta=0$ Eq. (8) exactly matches with Eq. (9) of Nandeppanavar et al. [17] when $n=\lambda=1$ in their model. Considering $\Pr=1$, $A=B=0.1$ they have calculated $-\theta'(0)=0.864169$ which is in very good agreement with our calculated value 0.86423064 when $S=0$, $\lambda=1$, $\beta=0$, $\Pr=1$, $A=B=0.1$. The afore-mentioned results give us confidence to use the present numerical code.

Results and Discussion

The numerical simulation of Eqs. (7) to (8) subject to the boundary conditions (15) are carried out for various values of the physical parameters S, β, λ, A, B and λ for obtaining the condition under which the dual (upper and lower branch) solutions for the unsteady flow over a shrinking sheet may exist. In Figs. 2 to 7, we have investigated the variation of the reduced skin friction coefficient $\mathrm{Re}_x^{1/2}C_f=f''(0)$, and the local Nusselt number or reduced heat transfer from the surface of the sheet $\mathrm{Re}_x^{-1/2}Nu_x=-\theta'(0)$ to the fluid for different values of s, β, and λ keeping the values of the other parameters $A=B=0.2$, and $\Pr=0.71$ fixed. These figures show that the number of solutions depend on the suction parameter S, unsteadiness

parameter β, and shrinking parameter λ. From Figs. 2 and 3 we notice that for a shrinking sheet ($\lambda = -1$) there are two solutions (dual) when $S_c < S \le S_s$ where $S_c = 2.1106$ and $S_s = 2.5110$ are respectively the critical suction parameters corresponding to the upper and lower branch solutions. Here the solid line represents the upper branch solution whereas the dotted one for the lower branch solution. For $S < S_c$ there exists no solution at all whereas at $S = S_c$ there is only one solution. On the other hand for $S > S_s$, we found only the upper branch solution. The upper branch solution increases with the increase of S whereas the lower one decreases with the increase of S. Miklavčič and Wang [8] have studied the steady viscous (Newtonian) fluid flows over a permeable linearly shrinking surface and have shown that suction at the wall will generate dual solutions only when the suction parameter S is greater than or equal to 2. It is good to mention that Miklavčič and Wang [8] have identified only S_c but not S_s. Our calculated value of $S_c = 2.1106$ is slightly higher than the value of Miklavčič and Wang [8]. We have investigated these features (higher S_c and existence of S_s) in details and identified that unsteadiness is the factor behind these.

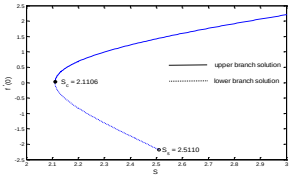

Figure 2. Values of $f''(0)$ versus S when $\lambda = -1$, $\beta = -2$, $A = 0.2$, $B = 0.2$, and $\Pr = 0.71$.

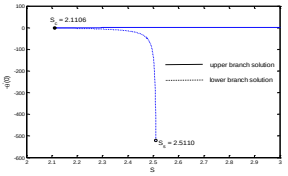

Figure 3. Values of $-\theta'(0)$ versus S when $\lambda = -1$, $\beta = -2$, $A = 0.2$, $B = 0.2$, and $\Pr = 0.71$.

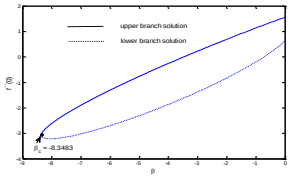

Figure 4. Values of $f''(0)$ versus β when $\lambda = -1$, $s = 2.2$, $A = 0.2$, $B = 0.2$, and $\Pr = 0.71$.

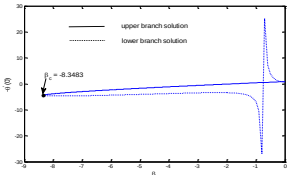

Figure 5. Values of $-\theta'(0)$ versus β when $\lambda = -1$, $s = 2.2$, $A = 0.2$, $B = 0.2$, and $\Pr = 0.71$.

In Figs. 4 and 5 we have plotted the values of $f''(0)$ and $-\theta'(0)$ against β for a shrinking sheet ($\lambda = -1$) when $S = 2.2$, $A = B = 0.2$ and $\Pr = 0.71$. Here we identified the critical β_c for the existence of the dual solutions. These figures indicate that dual solutions exist when $-8.3483 \approx \beta_c < \beta \le 0$. At $\beta = \beta_c$ there exists only one solution whereas for $\beta < \beta_c$ no solution can be found. The reduced skin friction coefficient increases with the increase of the unsteadiness parameter for both the upper and lower branch solutions. For the upper branch solution these values are higher than those of the lower branch solution. For the upper branch solution the reduced Nusselt number increases with the increase of β. On the other hand the reduced Nusselt number for the lower branch solution shows some unusual oscillation. Rahman et al. [14] done the stability analysis for a nanofluid flow and found that the upper branch solution is stable and physically acceptable whereas the lower branch solution is unstable and physically not acceptable. This result is well established and has not been repeated here for brevity.

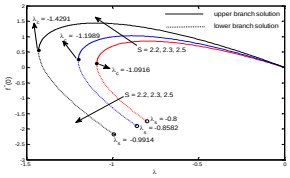

Figure 6. Values of $f''(0)$ versus λ for different values of s when $A = 0.2$, $B = 0.2$, and $\Pr = 0.71$.

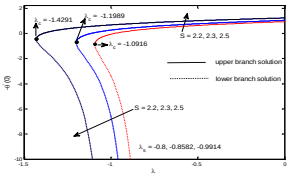

Figure 7. Values of $-\theta'(0)$ versus λ for different values of s when $A = 0.2$, $B = 0.2$, and $\Pr = 0.71$.

The variations of $f''(0)$ and $-\theta'(0)$ against λ for different values of S are depicted in Figs. 6 and 7, respectively when $\beta = -2$, $A = B = 0.2$, and $\Pr = 0.71$. In these figures we have calculated the critical λ for various values of S. From these figures we notice that, there are two solutions when $\lambda_c < \lambda \le \lambda_s$, one solution when $\lambda = \lambda_c$ and $\lambda > \lambda_s$, and no solution when $\lambda < \lambda_c$, where λ_c and λ_s are the critical values of λ corresponding to the upper and lower branch solutions. Thus, for $\lambda < \lambda_c$ the full Navier-Stokes equations and energy equation need to be solved. The critical values of λ_c are -1.0916, -1.1989, -1.4291 for $s = 2.2$, 2.3, 2.5 while the corresponding λ_s are -0.8, -0.8582, -0.9914. Thus, both $|\lambda_c|$ and $|\lambda_s|$ increases with the increase of S that is application of suction at the surface broadens the solution space for the existence of the dual solutions. The values of $f''(0)$ and $-\theta'(0)$ increase with the increase of S for the upper branch solution whereas they decrease for the lower branch solution for the increase of S. We also notice that for a fixed value of the other parameters the reduced skin friction coefficient for the upper branch solution first increases with the increase of λ within the region $\lambda_c \le \lambda \le \lambda_1$(say) then it decreases with the further increase of λ. On the other hand values of $f''(0)$ decrease with the increase of λ for the lower branch solution. Figure 7 depicts that values of $-\theta'(0)$ for the upper branch solution increase with the increase of λ whereas for the lower branch solution these values decrease with the increase of λ.

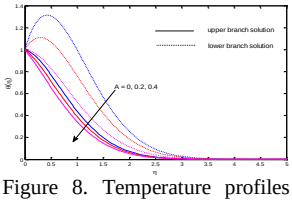

Figure 8. Temperature profiles for different values of A when $\lambda = -1$, $\beta = -2$, $s = 2.2$, $B = 0.2$, and $\Pr = 0.71$.

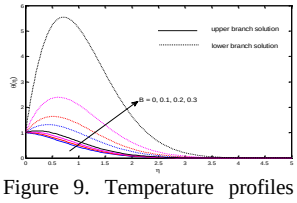

Figure 9. Temperature profiles for different values of B when $\lambda = -1$, $\beta = -2$, $s = 2.2$, $A = 0.2$, and $\Pr = 0.71$.

The effects of the space dependent heat source parameter A and the temperature dependent heat source parameter B on the nondimensional temperature profiles are depicted in Figs. 8-9, respectively. Figure 8 reveals that nondimensional temperature profiles decrease hence the thickness of the thermal boundary layer also decrease with the increase of A. On the other hand an opposite behavior of B on the temperature profiles is observed as can be seen from Fig. 9. Owing to the presence of temperature dependent heat generation it is apparent that there is an increase in the thermal state of the fluid. Hence from Fig. 9 we observe that temperature increases as $B(>0)$ increases.

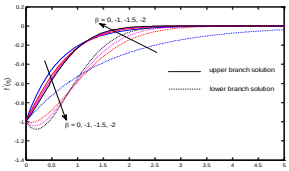

Figure 10. Velocity profiles for different values of β when $\lambda=-1$, $s=2.2$, $A=B=0.2$, and $\Pr=0.71$.

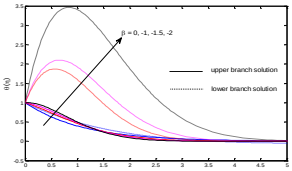

Figure 11. Velocity profiles for different values of β when $\lambda=-1$, $s=2.2$, $A=B=0.2$, and $\Pr=0.71$.

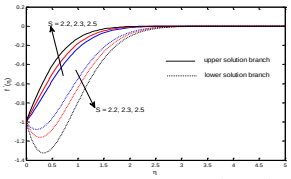

Figure 12. Velocity profiles for different values of S when $\lambda=-1$, $\beta=-2$, $s=2.2$, $A=0.2$, $B=0.2$ and $\Pr=0.71$.

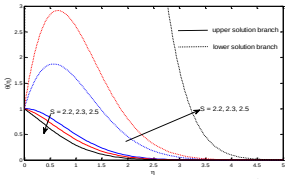

Figure 13. Temperature profiles for different values of S when $\lambda=-1$, $\beta=-2$, $s=2.2$, $A=0.2$, $B=0.2$ and $\Pr=0.71$.

The effect of the unsteadiness parameter for a decelerating shrinking sheet ($\beta\le 0$) on the velocity and temperature distributions are shown in Figs. 10-11, respectively. Figure 10 shows that fluid velocity near the surface of the sheet increases with the increase of the magnitude of β for both the upper and lower branch solutions. But away from the surface of the sheet where inertia forces are dominant compared to the viscous forces these profiles overlap. For sufficiently large $|\beta|$ boundary layer separates from the surface of the sheet for the lower branch solution as a consequence back flow occurs. The temperature of the fluid within the boundary layer for the upper branch solution increases near the surface of the sheet with the increase of $|\beta|$ (Fig. 11). Away from it these profiles overlap and decrease with the further increase of $|\beta|$. The temperature corresponding to the lower branch solution increases with the increase of $|\beta|$ throughout the boundary layer. Figure 12 further reveals that the dimensionless velocity profile $f'(\eta)$ increases with the increasing values of the suction parameter for the upper solution branch and decreases with the suction parameter for the lower solution branch. It can be seen from Fig. 13 that temperature profiles $\theta(\eta)$ decrease with the increase of S for an upper solution branch and increase for a lower solution branch. The thickness of the thermal boundary layer for upper solution branch is smaller than the corresponding thickness of the lower solution branch. It is good to mention that the maximum of the temperature profiles for the lower branch solution increases quite rapidly with the increase of S. Thus, Fig. 13 is plotted within $0\le\theta(\eta)\le 3$ to magnify the solution as for large $\theta(\eta)$ the difference among the solutions is in distinguishable.

Conclusions

From the numerical simulations the critical suction, unsteadiness, and shrinking parameters have been identified for the existence of the dual solutions. For $S_c<S\le S_s$, $\lambda_c<\lambda\le\lambda_s$, and $\beta>\beta_c$ the solutions have two branches, namely, an upper branch and a lower branch. The existence of S_s and λ_s is due to the unsteadiness of the problem. For a steady case $S_s=\lambda_s=0$. The unsteadiness significantly controls the flow and heat transfer characteristics. The upper branch solution is stable whereas the lower branch solution is unstable. The temperature dependent heat source parameter intensifies the fluid temperature whereas space dependent heat source parameter reduces it within the boundary layer.

References

[1] Crane, L.J., Flow past a stretching plate, *J. Appl. Math. Phys*., (ZAMP), **21**, 1970, 645-647.

[2] Gupta, P.S. & Gupta, A.S., Heat and mass transfer on a stretching sheet with suction and blowing, *Can. J. Chem. Engng*., **55**, 1977, 744-746.

[3] Banks, W.H.H., Similarity solutions of the boundary-layer equations for a stretching wall, *J. Mech. Theor. Appl.*, **2**, 1983, 375-392.

[4] Macleod, B. & Rajagopal, K.R., On the uniqueness of the flow of a Navier-Stokes fluid due to stretching boundary, *Arch. Ration. Mech. Anal*., 98, 1987, 385.

[5] Liao, S.-J. & Pop, I., Explicit analytic solution for similarity boundary layer equations, *Int. J. Heat Mass Transfer*, **47**, 2004, 75-85.

[6] Ishak, A., Nazar, R. & Pop, I., Heat transfer over an unsteady stretching permeable surface with prescribed wall temperature, *Nonlinear Anal : Real World Appl*., **10**, 2009, 2909-2913.

[7] Wang, C.Y., Review of similarity stretching exact solutions of the Navier–Stokes equations, *Eur. J. Mech. B/Fluids*, **30**, 2011, 475–479.

[8] Miklavčič, M. & Wang, C.Y., Viscous flow due a shrinking sheet, Quart. Appl. Math., **64**, 2006, 283-290.

[9] Goldstein, J., On backward boundary layers and flow in converging passages, *J. Fluid Mech*., **21**, 1965, 33-45.

[10] Surma Devi, C.D., Takhar, H.S. & Nath, G., Unsteady, three-dimensional, boundary-layer flow due to a stretching surface, *Int. J. Heat Mass Transfer*, **29**, 1986, 1996-1999.

[11] Fang, T.-G., Zhang, J. & Yao, S.-S., Viscous flow over an unsteady shrinking sheet with mass transfer, *Chin. Phys. Lett*., **26**, 2009, 014703-1 – 014703-4.

[12] Zheng, L., Wang, L., Zhang, X., Analytic solutions of unsteady boundary flow and heat transfer on a permeable stretching sheet with non-uniform heat source/sink, *Commun. Nonlinear Sci. Numer. Simulat*., **16**, 2011, 731–740.

[13] Rahman, M.M. & Eltayeb, I.A., Radiative heat transfer in a hydromagnetic nanofluid past a nonlinear stretching surface with convective boundary condition, Meccanica, **48**, 2013, 601-615.

[14] Rahman, M.M., Rosca, A.V. & Pop, I., Boundary layer flow of a nanofluid past a permeable exponentially shrinking surface with second order slip using Buongiorno's model, *Int. J. Heat Mass Transfer*, **77**, 2014, 1133-1143.

[15] Shampine, L.F., Gladwell, I., & Thompson, S., Solving ODEs with MATLAB. Cambridge University Press (2003).

[16] Vajravelu, K., Viscous flow over a nonlinearly stretching sheet, *App. Math. Comput*., **124**, 2001, 281-288.

[17] Nandeppanavar, M.M., Vajravelub, K., Subhas Abel, M., Ng, C.-O, Heat transfer over a nonlinearly stretching sheet with non-uniform heat source and variable wall temperature, Int. J. Heat Mass Transfer, **54**, 2011, 4960–4965.